

**SENSORS**

# Skin-inspired quadruple tactile sensors integrated on a robot hand enable object recognition

Guozhen Li, Shiqiang Liu, Liangqi Wang, Rong Zhu\*

Robot hands with tactile perception can improve the safety of object manipulation and also improve the accuracy of object identification. Here, we report the integration of quadruple tactile sensors onto a robot hand to enable precise object recognition through grasping. Our quadruple tactile sensor consists of a skin-inspired multilayer microstructure. It works as thermoreceptor with the ability to perceive thermal conductivity of a material, measure contact pressure, as well as sense object temperature and environment temperature simultaneously and independently. By combining tactile sensing information and machine learning, our smart hand has the capability to precisely recognize different shapes, sizes, and materials in a diverse set of objects. We further apply our smart hand to the task of garbage sorting and demonstrate a classification accuracy of 94% in recognizing seven types of garbage.

Copyright © 2020  
The Authors, some  
rights reserved;  
exclusive licensee  
American Association  
for the Advancement  
of Science. No claim  
to original U.S.  
Government Works

**INTRODUCTION**

Multimodal tactile perception is important for achieving environment awareness, recognition of threats, and fine motor tasks. Skin-like delicate tactile abilities are of great importance to sophisticated applications of robots and prosthetics (1–5). Multisensing tactile sensors provide robots the ability to interact with its surroundings precisely, rapidly, and safely. Many researchers have proposed various tactile sensors based on piezoresistive (6), capacitive (7), triboelectric (8), electret (9), magnetic (10, 11), etc. Multisensory electronic skins (e-skins) have also been developed by directly integrating different sensors into a sensing network or array with stacking or planar structures (3, 12–15) or by using bespoke advanced materials and microstructures that are sensitive to physical stimuli (3, 16–20). Although the development of tactile sensors and e-skins has achieved notable progress, they still require complicated structures and fabrication schemes (21) and usually suffer from the problem of mutual interference when perceiving multiple stimuli at the same time (21, 22). We have previously reported thermosensation-based sensors and e-skin to perceive multiple stimuli using a planar array of thermistors (23) and used the sensors on a robotic hand to recognize objects (24). However, the integration of multiple sensors remains a challenge. Various physical stimuli exerted at the same position can be perceived by human skin owing to its embedded dense receptors; however, replicating this behavior in artificial sensors remains unrealized. A limited integration of sensors degrades the spatial resolution of tactile perception and restricts sensor application.

Tactile perception is useful in robotics for object recognition or grasping tasks. Existing tactile object recognition is mostly based on pressure/force sensing. However, for complex object recognition, e.g., garbage sorting, pressure/force sensing is not sufficient. Substances with similar mechanical features, e.g., fruit peel and fabric with similar softness, cannot be differentiated by only contact pressure. Different materials have different thermal conductivities. Combining the thermal property with mechanical features of an object enables enhanced recognition accuracy. Here, we propose a quadruple tactile sensor with the integration of pressure sensing, material thermal con-

ductivity sensing, and bimodal temperature (object temperature and environment temperature) sensing for the robot hand to precisely recognize objects (movie S1).

**RESULTS**

Human skin is endowed with sensitivities to various stimuli, such as contact pressure, temperature, and material texture, owing to its delicate sensory receptors in its unique epidermal and dermal microstructures (25, 26). We propose a flexible quadruple tactile sensor with skin-inspired multilayer microstructure (Fig. 1A). Thermosensitive ribbons deposited on a polyimide substrate are used to emulate thermoreceptors of human skin. Using uniform sensing elements to perceive thermal conductivity of object, measure contact pressure, as well as sense object temperature and environment temperature, the proposed sensor has multisensory integration, simple structure, and low cross-coupling. As illustrated in Fig. 1B, the quadruple tactile sensor is composed of two sensing layers sandwiching a porous silver nanoparticle-doped polydimethylsiloxane (PDMS) (fig. S4A). Each sensing layer consists of two sensing elements (called hot film and cold film) that are concentric annular chrome/platinum (Cr/Pt) thin films (Fig. 1B, inset) deposited on a flexible polyimide substrate and covered by a parylene encapsulation membrane as the protective layer (fig. S4B). The concentric annular design for the hot film and cold film works to eliminate temperature drift and bending/stretching strain in the sensor (27). The central sensing element has a lower resistance than the circumjacent sensing element. Under an equal applied voltage, the center element with a low resistance bears a large electric power, thereby is heated to a predefined higher temperature, and works as a hot film. The circumjacent sensing element with a large resistance bears a low Joule heating and works as a cold film. The hot films on the top and bottom sensing layers generate local thermal fields in their surroundings (Fig. 1C, ii). When an object contacts and presses the sensor, it contacts the top sensing layer, and the conductive heat transfer from the top hot film to its surrounding changes with the thermal conductivity of the object (Fig. 1C, iii). In other words, the top hot film responds to the thermal conductivity of the contact object (note S1). Therefore, the thermal conductivity of the object can be detected by the top hot film of the sensor, which provides a means to identify material because different materials have

State Key Laboratory of Precision Measurement Technology and Instruments, Department of Precision Instrument, Tsinghua University, Beijing 100084, China.

\*Corresponding author. Email: zr\_gloria@mail.tsinghua.edu.cn

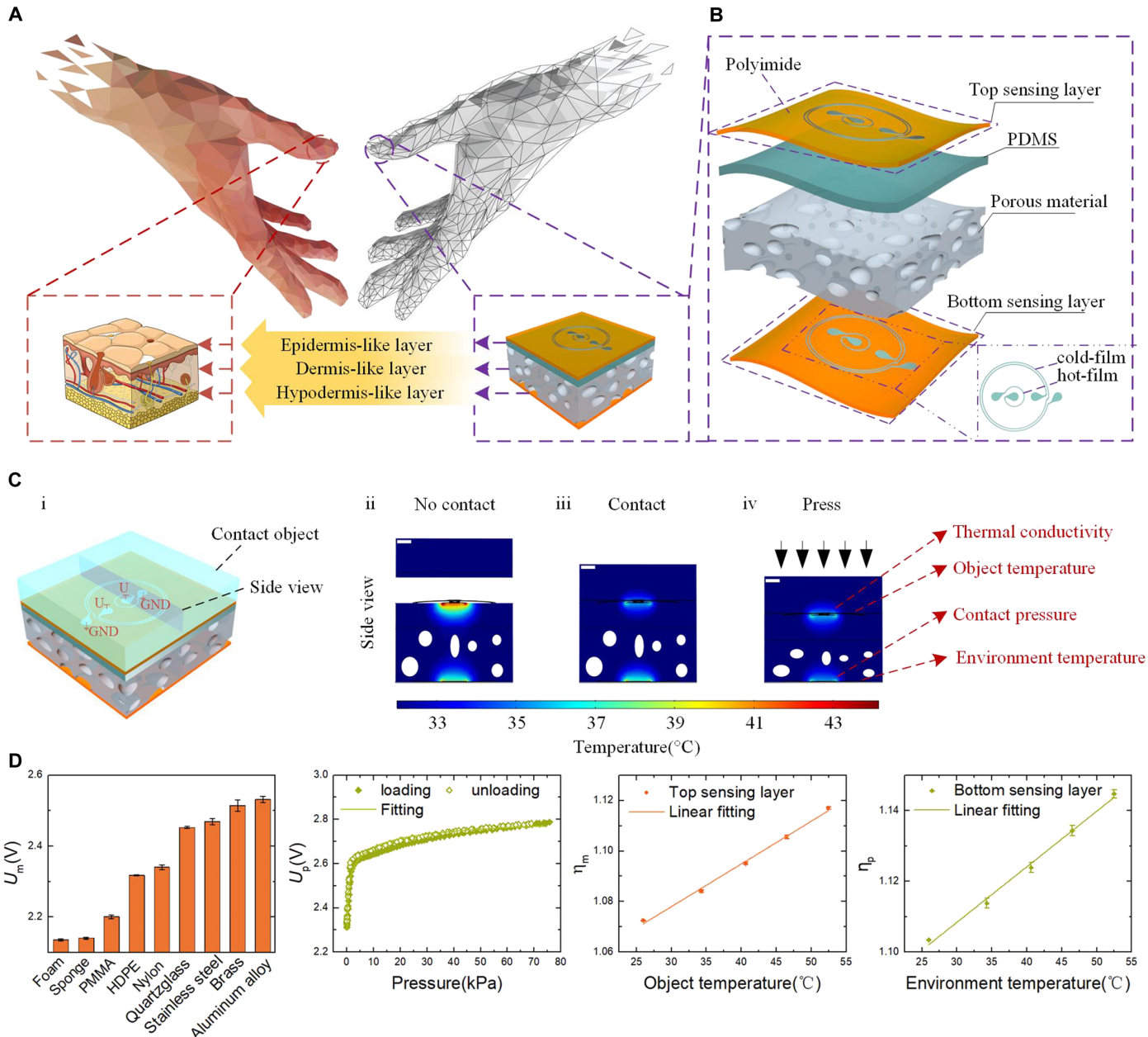


**Fig. 1. The structure, sensing principle and performance of the skin-inspired quadruple tactile sensor.** (A) The skin-inspired multilayer structure of quadruple tactile sensor. (B) Detailed structure of the sensor. (C) Working principles of sensor multisensing implementation are the following: (i) illustration of the sensor in contact with an object. (ii) Object is not in contact with the sensor. (iii) Object is in contact with the sensor, thereby the thermal field around the top hot film changes because of the heat transfer to the object. (iv) The functional porous material of the sensor is pressed and deformed, which increases its thermal conductivity, so as to enhance the heat transfer from the bottom hot film to the porous material. The sensor realizes multiperceptions by uniform thermosensation. Scale bars, 1 mm. GND, ground; U, applied voltage. (D) Responses of the quadruple tactile sensor to contact materials with different thermal conductivity (table S1), contact pressure, object temperature, and environment temperature, respectively. Three consecutive load-unloading measurements are conducted and shown in pressure responses.  $U_m$ ,  $U_p$ ,  $\eta_m$ , and  $\eta_p$  are denoted as the output signals of the sensor corresponding to contact matter, contact pressure, object temperature, and environment temperature, respectively. The output signals of the sensor are defined in the Supplementary Materials. The details of the conditioning circuit for the outputs of the sensor are described in fig. S5.

different thermal conductivities (28). Simultaneously, the pressure exerting on the sensor generates an elastic deformation of the porous material. The deformation increases the thermal conductivity of the porous material due to its piezothermic transduction (29), which enhances the conductive heat transfer from the bottom hot film to its surrounding (Fig. 1C, iv). That is, the contact pressure can be de-

tected by the bottom hot film of the sensor (note S2). The integrated circumjacent cold films on two sensing layers work as local temperature sensors (note S3); specifically, the top cold film detects the object temperature, and the bottom cold film detects the temperature on the bottom layer (approximate to environment temperature). The design of the central hot film and circumjacent cold film represents

a trade-off between the sensitivity and the dimension of the sensor. The space between the hot film and the cold film integrated on the same sensing layer is designed to avoid thermal interference from the hot film to the cold film. By lowering the predefined heating temperature of the hot film, the space between the hot film and the cold film can be reduced; however, the sensitivity of the sensor is also reduced. An alternative way to reduce the dimension of the sensor but not lose its sensitivity is to downsize the hot film and the cold film.

Two sensing layers of the quadruple tactile sensor are connected into two respective Wheatstone bridge feedback circuits for their signal conditionings (fig. S5). The hot film and cold film on each sensing layer are placed, respectively, into two legs of one Wheatstone bridge. The bridge circuit is balanced by a constant temperature difference (CTD) feedback circuit. The top voltages of the bridges for the top and bottom sensing layers (denoted as  $U_m$  and  $U_p$ , respectively) are defined as outputs of the sensor corresponding to thermal conductivity of object and contact pressure, respectively. The ratios of cold-film voltages to configuration resistor voltages for the top and bottom sensing layers [denoted as  $\eta_m = U_{mc}/(U_m - U_{mc})$ ,  $\eta_p = U_{pc}/(U_p - U_{pc})$ , where  $U_{mc}$  and  $U_{pc}$  refer to the cold-film voltages of top and bottom sensing layers, respectively] are defined as outputs of the sensor corresponding to object temperature and environment temperature, respectively. Using the CTD feedback circuits and the cold films, the hot films achieve temperature compensations (30). Therefore, the perceptions of contact pressure and thermal conductivity of object are not susceptible to temperature variation (fig. S6 and note S4). In addition, bending compensation is also achieved by adopting a concentric annular configuration for hot films and cold films of the quadruple tactile sensor that ensures that the object material sensing and contact pressure sensing of the sensor are not susceptible to bending strain (note S4) (27). A layer of pure PDMS is placed underneath the top sensing layer to avoid mutual interference between the top and bottom sensing elements. The quadruple tactile sensor capably perceives the thermal conductivity of an object, measures contact pressure, as well as senses object temperature and environment temperature simultaneously and independently. Figure 1D illustrates the responses of the quadruple tactile sensor to the objects with different thermal conductivities (table S1), contact pressures, object temperatures, and environment temperatures, respectively. The results show the performances of the sensor in discriminating materials, detecting contact pressures with a high sensitivity in initial contact (<2.5 kPa, 117 mV/kPa) and a low hysteresis error of 2.5% and sensing object temperatures and environment temperatures with sensitivities of 0.0017 and 0.0016°C<sup>-1</sup>, respectively.

Simultaneous and independent detections of multiple stimuli are necessary in practical applications. Figure 2A shows the result of the quadruple tactile sensor in simultaneously detecting object temperature and object material, and Fig. 2B shows simultaneously detecting environment temperature and contact pressure. The results indicate that the quadruple tactile sensor can detect object temperature and identify material type (by its thermal conductivity) simultaneously with a low cross-coupling error of less than 3.4%. The sensor also demonstrates simultaneous detections of environment temperature and contact pressure with low cross-coupling errors of less than 3.8% for pressure sensing and less than 4.2% for temperature sensing. In addition, to further evaluate the simultaneous detections of contact material and contact pressure, we put different materials onto the quadruple tactile sensor and pressed them using a force gauge. Figure 2 (C and D) shows detection results with low cross-coupling errors of

less than 2.6% for material sensing and less than 4.5% for pressure sensing. Figure 2E further demonstrates continuous detections of material (by its thermal conductivity), contact pressure, and object temperature and environment temperature using the quadruple tactile sensor. When placing a polymethyl methacrylate (PMMA) onto the sensor, there is an air gap at the interface between the PMMA and the sensor due to nonideal contact. When loading a pressure onto the PMMA, the pressing force pushes the PMMA in tight contact with the sensor; therefore, the output signal  $U_m$  of the material thermal conductivity changes slightly after applying pressure. The experiment results verify that low cross-couplings among multimodal sensors can be achieved. This is essential for simultaneous detections of multiple stimuli. The stability and durability of the quadruple tactile sensor were further evaluated. Figure S7A illustrates the responses of the quadruple tactile sensor to alternately loading and unloading pressure between 0 and 20 kPa onto the sensor for 500 continuous cycles, which validates the good stability and durability of the sensor.

The human hand has the ability to recognize objects with different sizes, shapes, and materials by means of thermoreceptors and mechanoreceptors in skin. Motivated by this, here, we propose a humanoid robot hand integrated with quadruple tactile sensors to recognize sizes, shapes, and materials of objects by grasping. We incorporate material thermal conductivity sensing with pressure sensing and temperature sensing and, thus, combine mechanical features with thermal properties to improve object recognition accuracy. After investigating the most frequently contacted positions on the robot hand when it grasps diverse objects, we mounted 10 quadruple tactile sensors on five fingertips and the palm of the humanoid robot hand as shown in Fig. 3A. The output signals of 10 sensors were normalized (see Materials and Methods for details) and then converted into a 4 × 10 signal map as shown in Fig. 3A, where four rows of the signal map from top to bottom represent the output signals of the tactile sensors corresponding to the object temperature, environment temperature, thermal conductivity of object, and contact pressure. To train the object recognition ability of the robot hand, we operated the robot hand at room temperature to grasp a human hand and 12 other standard objects with different sizes (small and big), different shapes (cube and ball), and different materials [steel, acrylonitrile butadiene styrene (ABS), and sponge] (fig. S8A) and recorded the output signals of the quadruple tactile sensors when the robot hand grasped these objects. Different orientations and locations were considered in grasping objects. Figure 3B shows an example set of normalized signal maps of the tactile sensors when the robot hand grasped these objects. Notable differences were observed in these signal maps when the robot hand grasped the objects with different shapes (e.g., big steel cube and big steel ball), different sizes (e.g., big steel cube and small steel cube), or different materials (e.g., big steel cube, big ABS cube, and big sponge cube) and a human hand. Figure S8B presents more examples of normalized signal maps of the robot hand in grasping objects from different orientations or at different locations. The output signals of the sensors exhibited scattering even in grasping the same object because of uncertainty of grip in orientation or location. A precise measurement relies on accurate placement of the sensor on an object, i.e., the sensor needs to tightly contact the object. However, in practice, grasping an object with unknown size, shape, and material involves uncertainty and nonideal conditions. Inspired by a human hand perceiving and recognizing objects, taking multisensory information from

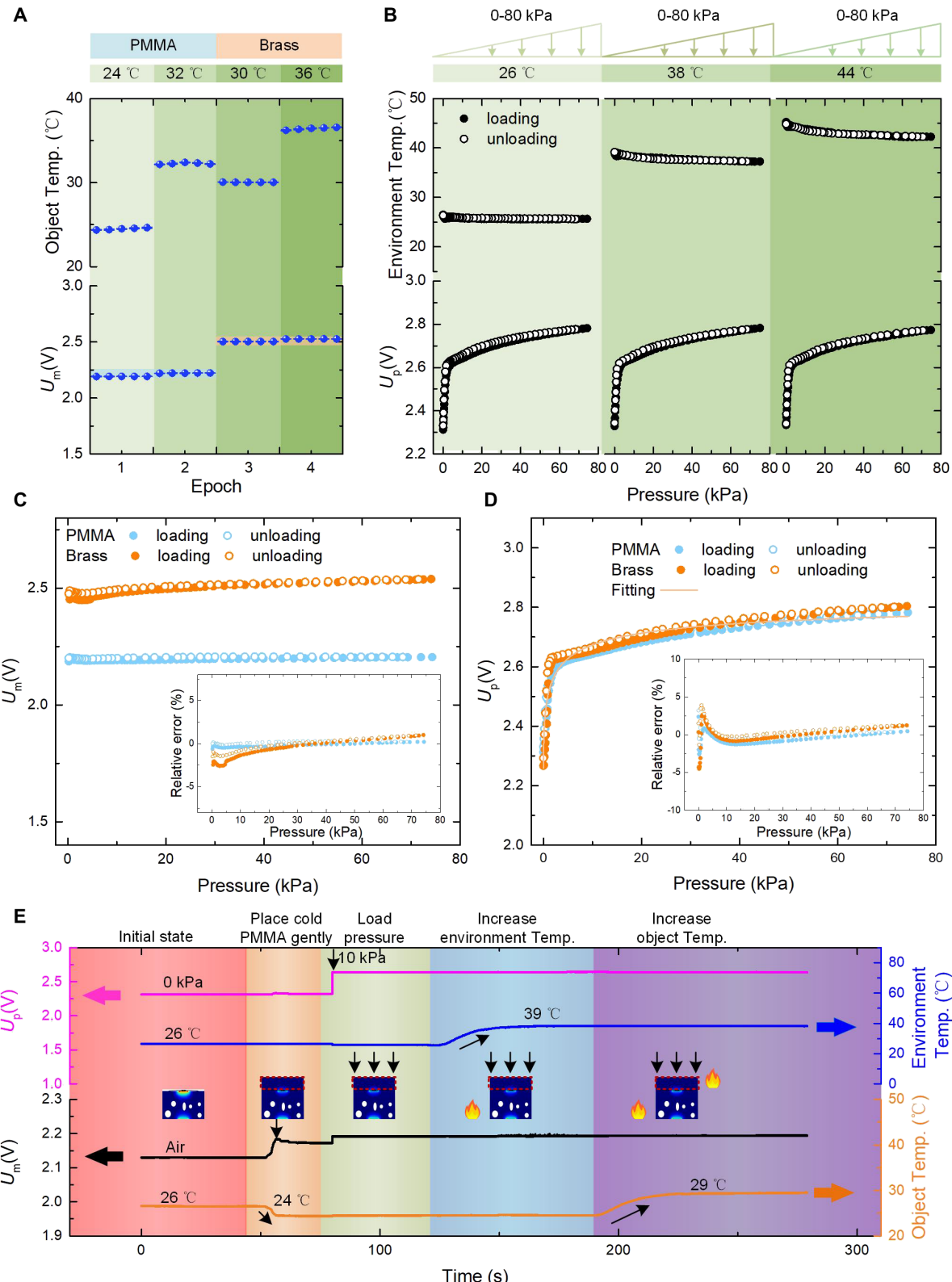


**Fig. 2. Multimodal sensing capability of the quadruple tactile sensor.** (A) Simultaneous and independent detections of object temperature (top) and object material (bottom). (B) Simultaneous and independent detections of environment temperature (top) and contact pressure (bottom). (C and D) Simultaneous and independent detections of contact material (by its thermal conductivity) and contact pressure. (E) Thermal conductivity detections of two materials (PMMA and brass) under different contact pressures. (D) Pressure detections under different contact materials. (E) Continuous detections of material (by its thermal conductivity), contact pressure, as well as object temperature and environment temperature.

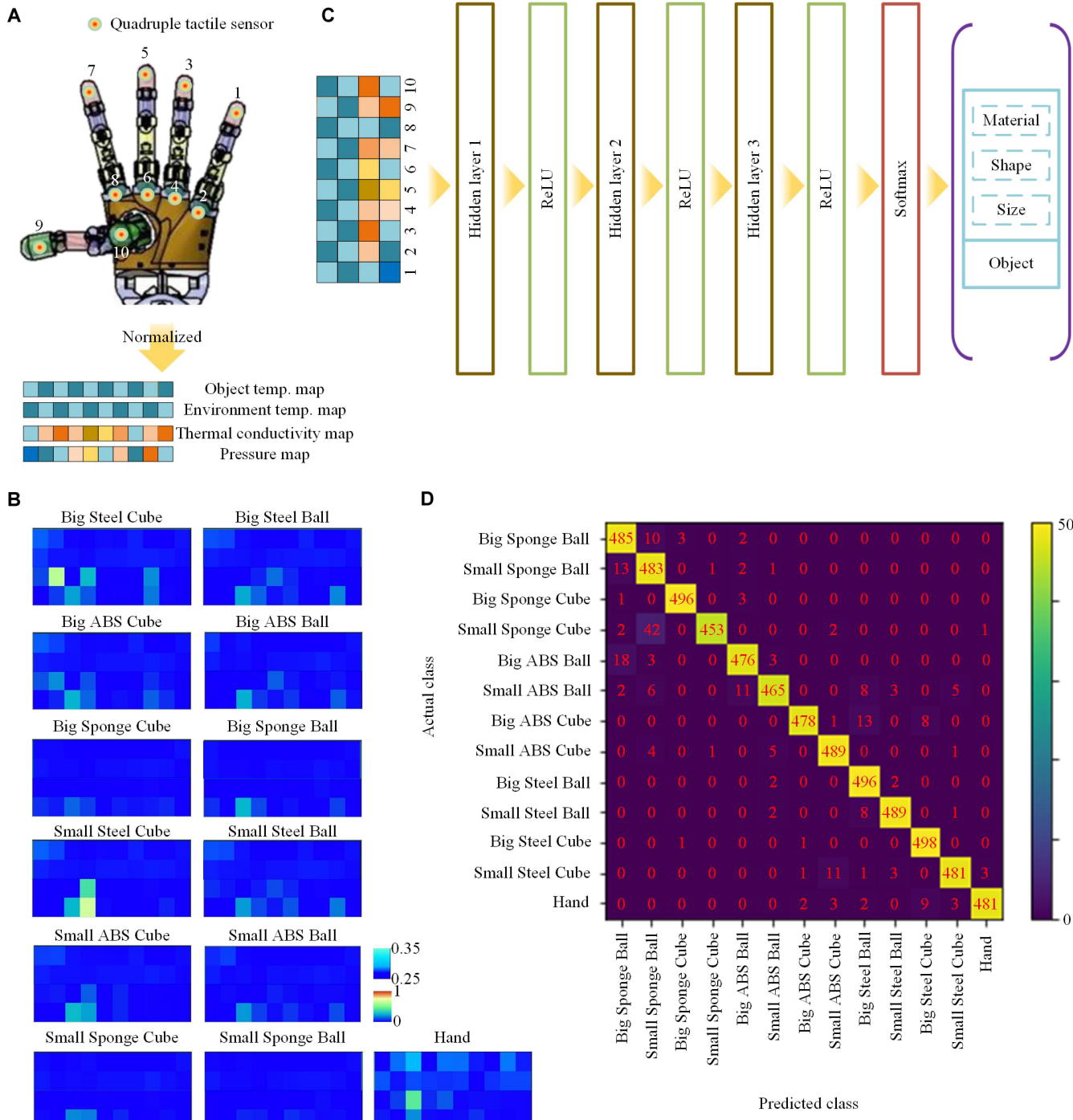


**Fig. 3. The robotic hand integrated with 10 quadruple tactile sensors for multiperceptions and object classification.** (A) Schematic diagram of the robot hand integrated with 10 quadruple tactile sensors and corresponding normalized signal maps of the sensors. (B) A typical example set of the normalized signal maps of the sensors. (C) Schematic diagram of the multilayer perceptron model structure for identifying object material, shape, and size. (D) Classification test confusion matrix with 6500 groups of the test dataset; each row and column represents an instance in a predicted class and an actual class, respectively, and the diagonal values represent correct results. The color bar represents the amount of the predicted number.

thermoreceptors and mechanoreceptors of fingers and palm into account enables accurate object recognition and precise identification of object size, shape, and material.

Incorporating neural networks and deep learning with tactile sensors to create robotic perception and recognition is an effective approach in the context of robotics for solving classification problems

without an explicit model (31, 32). In addition to mechanical sensing, we combined mechanical features with thermal properties of materials to identify objects. A multilayer perceptron (MLP) (33) that contains three hidden layers based on the PyTorch framework (34) shown in Fig. 3C was constructed to recognize objects with diverse sizes, shapes, and materials. The normalized signal map of the quadruple tactile sensors on the robot hand was used as the inputs of the MLP, and the outputs were the predicted size, shape, and material of the grasped object. Forty normalized signals of 10 quadruple tactile sensors on the five fingers and palm of the robotic hand were defined as a set of data. The dataset (containing 105,401 sets) of the normalized signal maps corresponding to a human hand and 12 standard objects with different sizes, shapes, and materials grasped from different orientations were used to train and optimize the MLP model (fig. S9 to S11). Afterward, we used another test dataset (containing 6500 sets, 500 sets for each object) of the normalized signal maps detected in other grasping task to verify the trained MLP model. Figure 3D illustrates the test verification result of the test dataset by comparing the predicted results with the actual objects. The verification results indicate that the total classification accuracy reaches about 96% in recognizing the objects with different sizes, shapes, and materials.

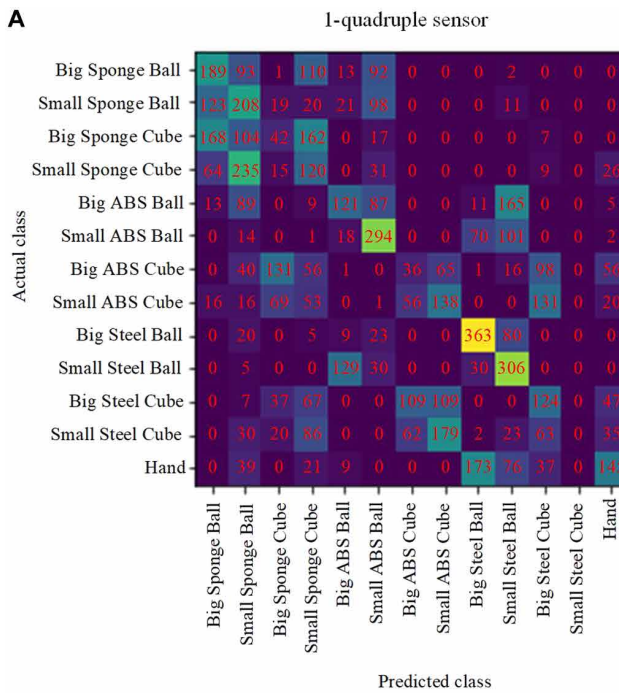
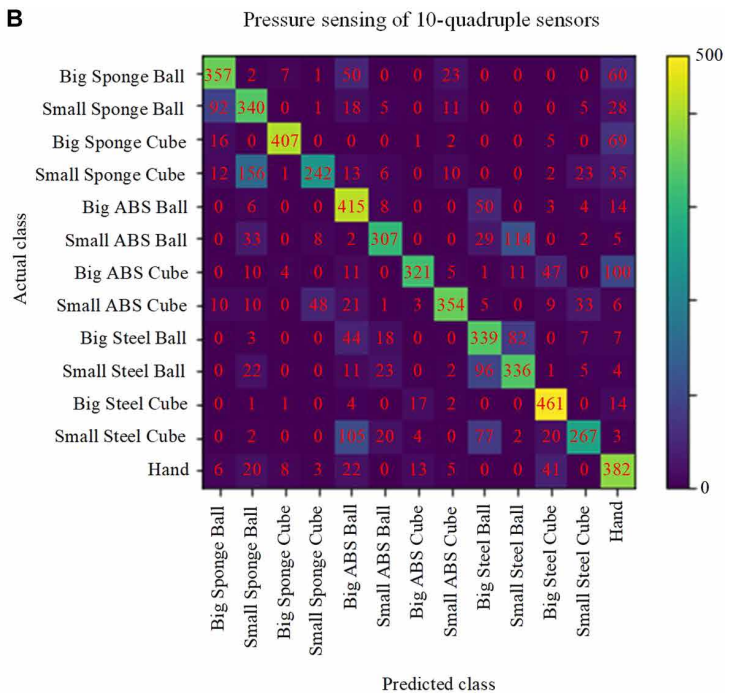
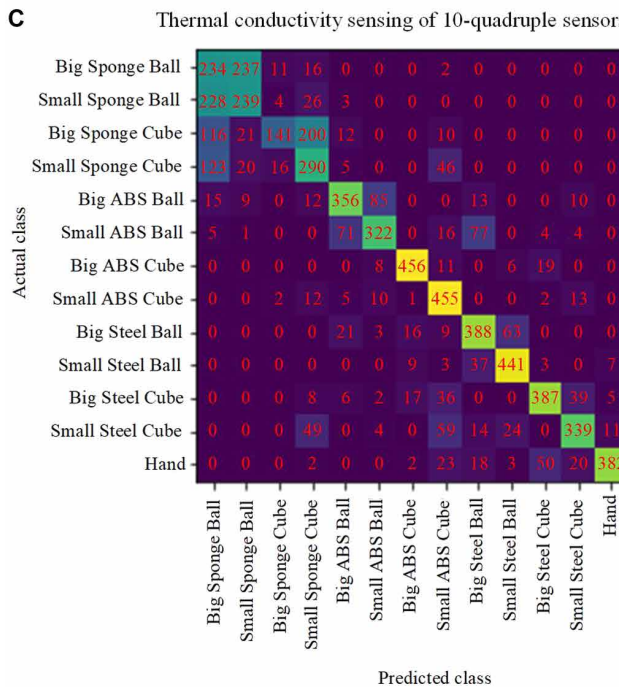
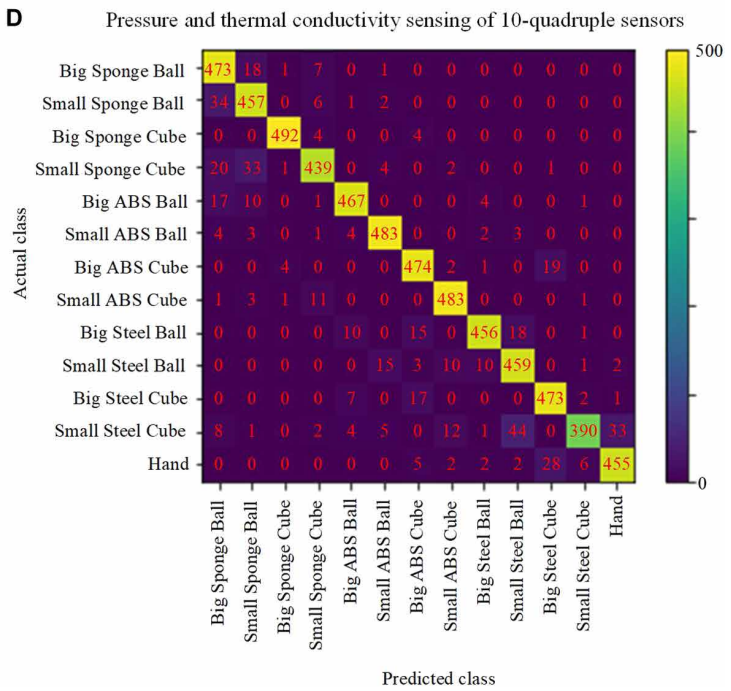
The integration of pressure sensing, material thermal conductivity sensing, and bimodal temperature (object temperature and environment temperature) sensing is important to achieve accurate object recognition. Figure 4 shows the classification results that use different configurations of the sensing data from the quadruple sensors to recognize objects. The classification model has the same structure (i.e., same number of hidden layers and neurons) as shown in Fig. 3C. Figure 4A demonstrates the classification result when using the dataset from one quadruple tactile sensor mounted on the middle fingertip of the humanoid robot hand. It is seen that using one sensor on a finger cannot accurately recognize object size and shape. The total classification accuracy using one sensor reaches about 32.1%. Variation of contact position or orientation of object influences the recognition accuracy when using only one sensor. In contrast, using multiple quadruple tactile sensors on the five fingers and palm for object recognition can achieve accurate recognition of shape, size, and material as shown in Fig. 3D. Figure 4 (B and C) shows the classification results that use only pressure sensing or only thermal conductivity sensing of 10 quadruple sensors to recognize objects. Using only pressure sensing in object classification cannot accurately discriminate objects with similar sizes, shapes, and softness but with different materials, e.g., a small ABS ball from a small steel ball. Therefore, the total classification accuracy using only pressure sensing reaches about 69.6% as shown in Fig. 4B. Using only thermal conductivity sensing in object classification cannot discriminate objects with similar materials and different shapes or sizes, e.g., a big sponge ball from a small sponge ball. The total classification accuracy using only thermal conductivity sensing reaches about 68.1% as shown in Fig. 4C. Combining pressure sensing with thermal conductivity sensing of 10 quadruple sensors can improve the classification accuracy that reaches about 92.3% as shown in Fig. 4D. However, there exists obvious misclassification between a human hand and other objects without temperature sensing. Some objects have temperature features besides material properties and geometrical features. For example, live animals have their own body temperatures, but inanimate objects do not. Some object temperatures vary with environment. Sensing object temperature and environment temperature allows more

accurate object recognition. Therefore, combining pressure sensing with thermal conductivity sensing and temperature sensing can greatly improve the accuracy of object classification; the total classification accuracy reaches about 96% in recognizing a human hand and other objects with different materials and different geometric features (sizes and shapes), as shown in Fig. 3D. Furthermore, the multisensory robot hand is used to grasp various objects with different sizes, shapes, and materials to recognize them in real time (movie S2) and to grasp objects from different orientations to recognize them in real time (movie S3). The multisensory robot hand is also used to intelligently identify whether the object is the target object as shown in movie S4. It is seen that the objects can be recognized accurately and quickly.

We applied the multisensory robot hand to a practical use. Garbage sorting is important to protect our living environment and contribute to green and sustainable development. Using robots to classify waste will help to ease the burden. We used the multisensory robot hand with quadruple tactile sensors to sort garbage. Seven types of recyclable/unrecyclable garbage (plastic bag, foam, carton, can, napkin, bread, and orange peel as shown in fig. S12A) that are common in daily life were used in experiments of garbage sorting. Garbage has diverse mechanical configurations, e.g., irregular crumpled plastic bag and rolled plastic bag, big cube-like bread and small hemisphere bread, and irregularly shaped orange peels. Figure 5A shows a set of normalized signal map examples of the robot hand when grasping these types of garbage. More signal map examples detected in grasping garbage with diverse materials, sizes, shapes, or orientations/locations are shown in fig. S12B. The output signals of the sensors exhibited scattering even in grasping the same garbage because of uncertainty of grip in orientation or position. The training dataset (containing 21,918 sets) of seven types of garbage was used to train the garbage classifier (Fig. 5B). Afterward, the trained garbage classifier was used to classify garbage type and identify recyclable or unrecyclable garbage. The corresponding confusion matrix of the test dataset (containing 1400 sets, 200 sets for each type of garbage) for garbage sorting is shown in Fig. 5C. The total classification accuracy in recognizing seven types of garbage reached about 94%, which indicates that it is feasible to use the multisensory robot hand to sort garbage. The smart robot hand was further used to identify recyclable and unrecyclable garbage in real time as shown in movie S5.

## DISCUSSION

Our results demonstrate the promising application of quadruple tactile sensors for improving tactile perception and object recognition. The proposed quadruple tactile sensor has the ability to simultaneously and independently perceive multiple stimuli—i.e., object material (by its thermal conductivity) and contact pressure, as well as object temperature and environment temperature—by using uniform and simple thermistors with low cross-coupling. The integration of multiple sensors with low cross-coupling is achieved in our quadruple tactile sensor design. Multiple quadruple tactile sensors provide tactile perception to a humanoid robot hand. The tactile sensing information is fused using machine learning to achieve precise object size, shape, and material recognition. In particular, different substances can be discriminated on the basis of their distinct thermal conductivities and mechanical features and thus improves the accuracy of object recognition. Multisensory capabilities of the robot hand can

**A****B****C****D**

**Fig. 4. Comparison of classification results when using different configurations of sensing data from quadruple sensors to recognize objects.** (A) Classification result when using data from only one quadruple sensor mounted on the middle fingertip. The total classification accuracy reaches about 32.1%. (B) Classification result when using only pressure sensing of 10 quadruple sensors. The total classification accuracy reaches about 69.6%. (C) Classification result when using only thermal conductivity sensing of 10 quadruple sensors. The total classification accuracy reaches about 68.1%. (D) Classification result when using combination of pressure sensing and thermal conductivity sensing of 10 quadruple sensors. The total classification accuracy reaches about 92.3%. The color bar represents the amount of the predicted number.

be used potentially for wide practical applications. We have demonstrated an application of our technology for garbage sorting. Moreover, we showcase garbage sorting with unseen objects in note S5. Our ap-

proach is to modify the garbage classifier by means of data augmentation of a training dataset with Gaussian noise to improve model generalization ability. Real-life garbage sorting is complicated, and

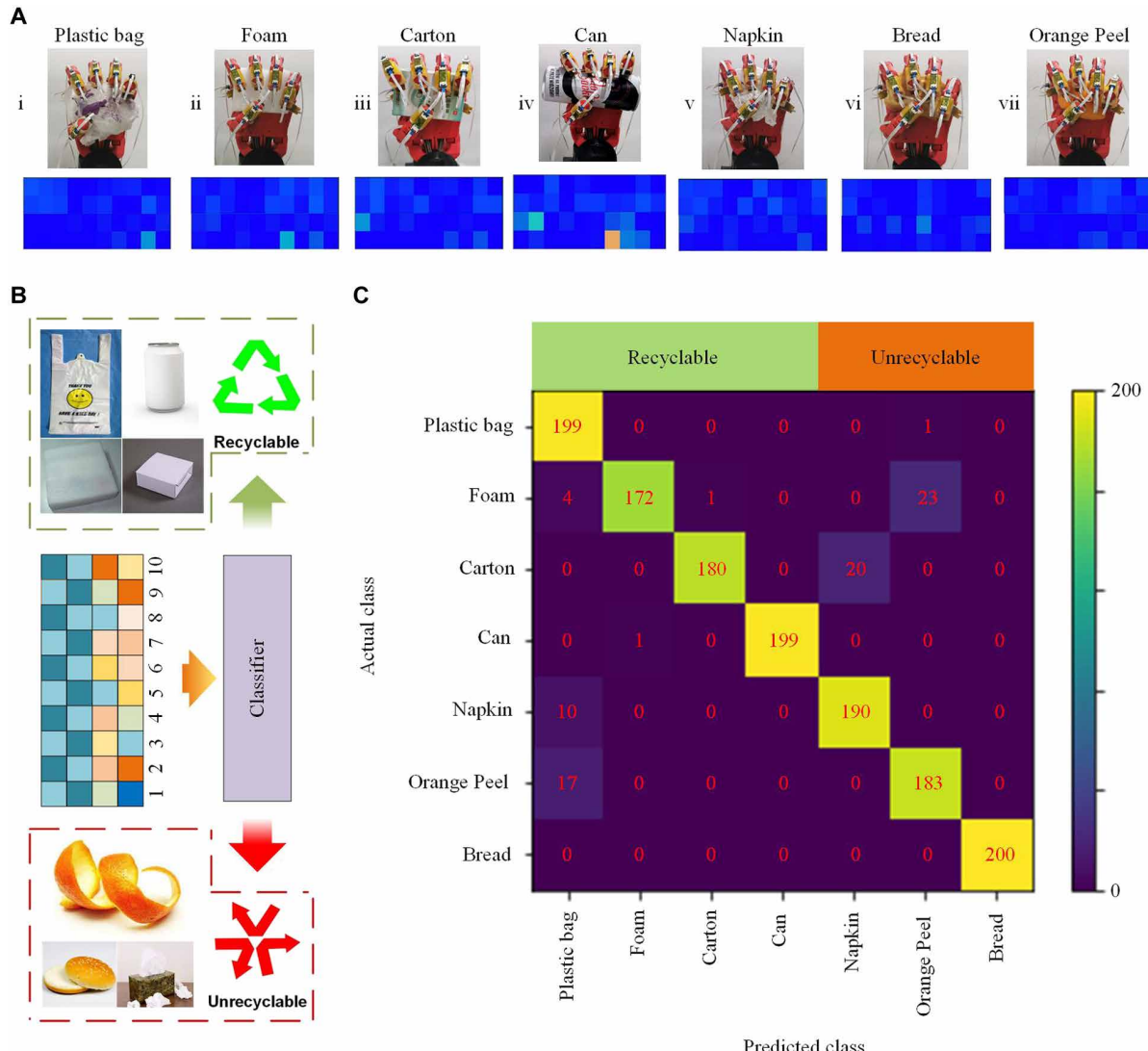


**Fig. 5. Robot hand integrated with quadruple tactile sensors for garbage sorting.** (A) A group of example signal maps when the robot hand grips seven types of garbage. (B) Schematic diagram of garbage sorting. (C) Classification test confusion matrix with 1400 groups of the dataset in recognizing seven garbage objects. The color bar represents the amount of the predicted number.

it is difficult to cover all aspects in experiments due to limited sample size. In this study, we selected seven types of garbage with different mechanical configurations to demonstrate the promising potential of the quadruple tactile sensor for robotic garbage sorting. For more realistic applications, however, further tests on a larger set of garbage and additional research on advanced learning algorithms still need to be conducted.

## MATERIALS AND METHODS

### Fabrication of thermal sensing layer

The thermal sensing layers of the quadruple tactile sensor were made by the following steps (27): (i) We spin-coated a 30- $\mu\text{m}$  photoresist (KXN5735-LO, Rdmicro Co. Ltd.) on a polyimide substrate (AP8525R, DuPont Co. Ltd.). (ii) We obtained the pattern by photolithography and development. (iii) We sputtered 30-nm-thick chromium as an adhesion layer and then sputtered 150-nm-thick platinum as the

thermosensitive layer. (iv) The patterned substrate was immersed in acetone for 2 hours to dissolve the photoresist and then washed with absolute ethanol and deionized water. (v) We deposited 4- $\mu\text{m}$ -thick polyethylene film on the patterned substrate as a protective layer.

### Fabrication of porous material

The porous material is made of PDMS (Sylgard 184, Dow Corning Company), citric acid monohydrate (CAM) particles, and silver nanoparticles (diameter of <100 nm; S110970, Aladdin Co. Ltd.) (24). PDMS was used as the base material in consideration of its excellent properties of elasticity, stability, easy fabrication, and adjustability. The ratios of components are a PDMS:cross-linker volume ratio of 10:1 weight %, a PDMS:CAM volume ratio of 1:3, and a silver nanoparticles volume ratio of 2 volume %. After fully stirring the mixture (10 min), we poured it into a PMMA mold and cured it at 75°C for 2 hours. After demolding, we immersed the material in ethanol for 24 hours to dissolve the CAM and form porosity and then washed it

with deionized water. Last, the porous functional materials were dried at 70°C for 1 hour.

### Fabrication of quadruple tactile sensor

The quadruple tactile sensor was made by the following steps: (i) A pure PDMS layer was cured in a thin PMMA mold (10 mm by 10 mm by 2 mm) at 75°C for 2 hours. (ii) We stacked another thick PMMA mold (10 mm by 10 mm by 4 mm) on the pure PDMS layer and fabricated porous material as described previously. (iii) After demolding and drying, we adhered the sensing layers to the upper surface of the PDMS layer and the lower surface of the porous material. The diagram of the corresponding fabrication process is shown in fig. S4D.

### Circuit design

As shown in fig. S5, the conditioning circuit of a quadruple tactile sensor was composed of two CTD circuits. The hot films and cold films were connected into Wheatstone bridges, and the differential voltages of both sensing layers were then amplified by amplifiers and fed back to the bridges for implementing the CTDs. The bridge top voltages and cold film voltages were further amplified by the voltage followers for sampling. The entire regulation circuit was integrated in a homemade printed circuit board.

### Experiment measurement and characterization on sensor performance

Pressure measurement was conducted by applying force on the quadruple tactile sensor using a mechanized z-axis stage (Handpi HLD) with a force gauge (Sundoo SH-50, 0.01 N of resolution). Temperature responses of the sensor were tested in a temperature-controlled oven (OGH60, Thermo Fisher Scientific Co. Ltd.). The quadruple tactile sensor was adhered onto a temperature-controlled plate to simulate environment temperature variation, and a pressure stimulus was applied onto the sensor via force gauge for testing simultaneous detections of pressure and environment temperature stimuli. The contact material adhered with a small temperature-controlled plate was used to conduct the simultaneous detections of material thermal conductivity and temperature stimuli. Two different materials (PMMA and brass) were used, and a pressure stimulus was applied onto the quadruple tactile sensor via force gauge for testing simultaneous detections of material thermal conductivity and pressure stimuli. Corresponding platform schematic of the sensor performance characterization is shown in fig. S4E. The intelligent robotic hand used a humanoid robotic hand (SCP-E5, Scramp Co. Ltd.) equipped with the quadruple tactile sensors.

### Selection of the installation positions on the robot hand for the quadruple tactile sensors

Before installing the quadruple tactile sensors on a robot hand, we used the robot hand to grasp various dye-coated objects and then recorded and counted the dyeing positions to determine the most frequently contacted sites on the robot hand as the sensor-mounted positions.

### Data acquisition and normalization

The multisensing signal of each sensor on the robotic hand was sampled by an analog-to-digital converter after being conditioned by the CTD circuit described above and then packaged and sent to a laptop through COM port (cluster communication port) for processing. Each set of data frame contains 40 signal values of 10 quadruple tactile sen-

sors mounted on the fingers and palm of the robot hand. Furthermore, the customized interactive control software programmed by LabVIEW (Laboratory Virtual Instrument Engineering Workbench) in a laptop disassembled and calculated the sensing data, and the corresponding pressure (denoted as  $P$ ), voltage related with object thermal conductivity (denoted as  $U_m$ ), object temperature (denoted as  $T_m$ ), and environment temperature (denoted as  $T_p$ ) perceived by each sensor were obtained and normalized to 0 to 1, respectively. Specifically, normalization was carried out by taking the maximum value of quantity as 1 and the minimum value as 0. Each row from bottom to top of the normalized map represents the pressure, thermal conductivity, environment temperature, and object temperature map of the matter being grasped. We defined 40 normalized signal values from 10 quadruple tactile sensors as a set of data. In recognizing 13 objects including 12 standard objects and a human hand, the total dataset (containing 111,901 sets) was acquired through grasping these objects about 20 times with different orientations and locations for each object, and each grasp action contained about 400 sets of data. The training and testing datasets for recognizing 12 standard objects and a human hand were randomly selected from the total dataset. In garbage sorting, the total dataset (containing 23,318 sets) was acquired through grasping garbage objects about 10 times with different orientations and locations for each object, and each grasp action contained about 300 sets of data. The training and testing datasets for garbage sorting were randomly selected from the total dataset.

### MLP model training and optimization

We implemented the MLP network for the humanoid robotic hand to conduct classification in the PyTorch framework. The MLP model has three fully connected hidden layers, and each hidden layer has 20 neurons. Rectified linear units (ReLU) were used into the MLP model to introduce nonlinearity. To optimize the MLP model, we set the learning rate of the model to 0.01, trained the network using the training dataset for 50 epochs with batches of 512 data samples, and presented the mean results over six test runs. We first set the number of hidden layers in the model to two and varied the number of neurons in the hidden layer to determine the appropriate number of neurons in the hidden layer. Figures S9A and S10 illustrate that the classification accuracy increases with the number of neurons but gradually saturates after the number of neurons is greater than 20. Therefore, we set the number of neurons in each hidden layer to 20. In addition, we further optimized the number of hidden layers of the model because the number of hidden layers also affects the classification accuracy. We set the number of hidden layer neurons to 20, then altered the number of hidden layers, and noticed the classification accuracy variation. The results shown in figs. S9B and S11 demonstrate that the classification accuracy reached its maximum when the number of hidden layers was three. Therefore, the optimized MLP structure has three hidden layers, and each hidden layer has 20 neurons.

### Operation and recognition of robot hand

The grasp action and applied pressure to hold an object for a robot hand (SCP-E5, Scramp Co. Ltd.) were automatically controlled by using its commercial robot controller (Scramp Co. Ltd.). The robot controller with the corresponding control algorithm (programmed in Codesys V3.5) controls the joints of the humanoid robotic hand to reach predefined target angles while monitoring that the joint torques do not exceed the predefined threshold.

Our customized interactive control software, programmed by LabVIEW and operated in a laptop, communicates with the robot controller through Object Linking and Embedding for Process Control Protocol (OPC) to command the robot hand to grasp the object. And then our customized interactive control software calls the trained MLP model programmed by Python (Python 3.7.0) and sends the normalized sensor signals to the MLP model for classifying the object.

The trained MLP model takes about 43 ms to figure out a classification result. Because the communication and call delay between software/hardware platforms is currently about 1 s in total, when the robot hand grasps an object, it usually takes about 1 s to recognize the object.

## SUPPLEMENTARY MATERIALS

[robotics.sciencemag.org/cgi/content/full/5/49/eabc8134/DC1](http://robotics.sciencemag.org/cgi/content/full/5/49/eabc8134/DC1)

Note S1. Theoretical analysis of thermal conductivity sensing mechanism.

Note S2. Theoretical analysis of pressure sensing mechanism.

Note S3. Temperature measurement principle by cold film.

Note S4. Temperature and bending compensation method.

Note S5. Garbage sorting with unseen objects.

Fig. S1. Spherical shell model and CTD conditioning circuit.

Fig. S2. Finite element method (FEM) simulation of porous material under different pressure.

Fig. S3. Results for garbage sorting with unseen objects.

Fig. S4. Composition of sensing layer and porous material, fabrication process, and sensor performance characterization platform schematic.

Fig. S5. The schematic of the sensor signals conditioning circuit.

Fig. S6. Temperature effects on material thermal conductivity and pressure detections of the quadruple tactile sensor.

Fig. S7. Quadruple tactile sensor repeatability and durability test and step response of pressure sensing.

Fig. S8. The objects used in the recognition experiment and more signal map examples.

Fig. S9. MLP optimization.

Fig. S10. Optimizing results of the MLP model with different neurons number.

Fig. S11. Optimizing results of the MLP model with different hidden layers number.

Fig. S12. The garbage used in the garbage sorting experiment and more signal map examples.

Table S1. Thermal conductivities of the materials used in the experiment.

Table S2. Temperature coefficient resistances (TCRs) of hot films and cold films of all quadruple tactile sensors used to the humanoid robot hand.

Movie S1. Summary of the robot hand with quadruple tactile sensors.

Movie S2. Robot hand with quadruple tactile sensors grabs and identifies object size, shape, and material in real time, respectively.

Movie S3. Robot hand with quadruple tactile sensors grabs and identifies human hand and object with different orientations in real time.

Movie S4. Robot hand with quadruple tactile sensors continuously and intelligently identify whether a grip is the set target.

Movie S5. Robot hand with quadruple tactile sensors is used for garbage classification tasks.

References (35–37)

## REFERENCES AND NOTES

1. G. Cannata, M. Maggiali, G. Metta, G. Sandini, An embedded artificial skin for humanoid robots, in *2008 IEEE International Conference on Multisensor Fusion and Integration for Intelligent Systems* (2008), pp. 434–438.
2. J. M. Romano, K. Hsiao, G. Niemeyer, S. Chitta, K. J. Kuchenbecker, Human-Inspired robotic grasp control with tactile sensing. *IEEE Trans. Robot.* **27**, 1067–1079 (2011).
3. S. Zhao, R. Zhu, Flexible electronic skin with multisensory integration. *Acta Chim. Sin.* **77**, 1250–1262 (2019).
4. Y. C. Lai, J. Deng, R. Liu, Y. C. Hsiao, S. L. Zhang, W. Peng, H. M. Wu, X. Wang, Z. L. Wang, Actively perceiving and responsive soft robots enabled by self-powered, highly extensible, and highly sensitive triboelectric proximity-and pressure-sensing skins. *Adv. Mater.* **30**, 1801114 (2018).
5. A. Chortos, J. Liu, Z. A. Bao, Pursuing prosthetic electronic skin. *Nat. Mater.* **15**, 937–950 (2016).
6. J. Kim, M. Lee, H. J. Shim, R. Ghaffari, H. R. Cho, D. Son, Y. H. Jung, M. Soh, C. Choi, S. Jung, K. Chu, D. Jeon, S. T. Lee, J. H. Kim, S. H. Choi, T. Hyeon, D. H. Kim, Stretchable silicon nanoribbon electronics for skin prosthesis. *Nat. Commun.* **5**, 5747 (2014).
7. N. C. Garcia, N. W. Taube, E. O. Polat, D. Ravinder, Energy-autonomous, flexible, and transparent tactile skin. *Adv. Funct. Mater.* **27**, 1606287 (2017).
8. Y. Cheng, D. Wu, S. Hao, Y. Jie, X. Cao, N. Wang, Z. L. Wang, Highly stretchable triboelectric tactile sensor for electronic skin. *Nano Energy* **64**, 103907 (2019).
9. S. Gong, J. Zhang, C. Wang, K. Ren, Z. L. Wang, A monocharged electret nanogenerator-based self-powered device for pressure and tactile sensor applications. *Adv. Funct. Mater.* **29**, 1807618 (2019).
10. Y. Z. Wu, Y. W. Liu, Y. L. Zhou, Q. K. Man, C. Hu, W. Asghar, F. L. Li, Z. Yu, J. Shang, G. Liu, M. Y. Liao, R. W. Li, A skin-inspired tactile sensor for smart prosthetics. *Sci. Robot.* **3**, eaat0429 (2018).
11. X. Yu, Z. Xie, Y. Yu, J. Lee, A. Vazquez-Guardado, H. Luan, J. Ruban, X. Ning, A. Akhtar, D. Li, B. Ji, Y. Liu, R. Sun, J. Cao, Q. Huo, Y. Zhong, C. Lee, S. Kim, P. Gutruf, C. Zhang, Y. Xue, Q. Guo, A. Chempakasseril, P. Tian, W. Lu, J. Jeong, Y. Yu, J. Cornman, C. Tan, B. Kim, K. Lee, X. Feng, Y. Huang, J. A. Rogers, Skin-integrated wireless haptic interfaces for virtual and augmented reality. *Nature* **575**, 473–479 (2019).
12. B. Xu, A. Akhtar, Y. Liu, H. Chen, W. H. Yeo, S. I. Park, B. Boyce, H. Kim, J. Yu, H. Y. Lai, S. Jung, Y. Zhou, J. Kim, S. Cho, Y. Huang, T. Bretl, J. A. Rogers, An epidermal stimulation and sensing platform for sensorimotor prosthetic control, management of lower back exertion, and electrical muscle activation. *Adv. Mater.* **28**, 4462–4471 (2016).
13. Q. L. Hua, J. L. Sun, H. T. Liu, R. R. Bao, R. M. Yu, J. Y. Zhai, C. F. Pan, Z. L. Wang, Skin-inspired highly stretchable and conformable matrix networks for multifunctional sensing. *Nat. Commun.* **9**, 244 (2018).
14. G. Cheng, E. Dean-Leon, F. Bergner, J. R. G. Olvera, Q. Leboutet, P. Mittendorfer, A comprehensive realization of robot skin: Sensors, sensing, control, and applications. *Proc. IEEE* **107**, 2034–2051 (2019).
15. Z. Huang, Y. Hao, Y. Li, H. Hu, C. Wang, A. Nomoto, T. Pan, Y. Gu, Y. Chen, T. Zhang, W. Li, Y. Lei, N. Kim, C. Wang, L. Zhang, J. W. Ward, A. Maralani, X. Li, M. F. Durstock, A. Pisano, Y. Lin, S. Xu, Three-dimensional integrated stretchable electronics. *Nat. Electron.* **1**, 473–480 (2018).
16. J. O. Kim, S. Y. Kwon, Y. Kim, H. B. Choi, J. C. Yang, J. Oh, H. S. Lee, J. Y. Sim, S. Ryu, S. Park, Highly ordered 3D microstructure-based electronic skin capable of differentiating pressure, temperature, and proximity. *ACS Appl. Mater. Interfaces* **11**, 1503–1511 (2018).
17. C. M. Boutry, M. Negre, M. Jorda, O. Vardoulis, A. Chortos, O. Khatib, Z. N. Bao, A hierarchically patterned, bioinspired e-skin able to detect the direction of applied pressure for robotics. *Sci. Robot.* **3**, eaau6914 (2018).
18. G. Y. Bae, J. T. Han, G. Lee, S. Lee, S. W. Kim, S. Park, J. Kwon, S. Jung, K. Cho, Pressure/temperature sensing bimodal electronic skin with stimulus discriminability and linear sensitivity. *Adv. Mater.* **30**, 1803388 (2018).
19. J. Park, M. Kim, Y. Lee, H. S. Lee, H. Ko, Fingertip skin-inspired microstructured ferroelectric skins discriminate static/dynamic pressure and temperature stimuli. *Sci. Adv.* **1**, e1500661 (2015).
20. S. M. Won, H. Wang, B. H. Kim, K. Lee, H. Jang, K. Kwon, M. Han, K. E. Crawford, H. Li, Y. Lee, X. Yuan, S. B. Kim, Y. S. Oh, W. J. Jang, J. Y. Lee, S. Han, J. Kim, X. Wang, Z. Xie, Y. Zhang, Y. Huang, J. A. Rogers, Multimodal sensing with a three-dimensional piezoresistive structure. *ACS Nano* **13**, 10972–10979 (2019).
21. J. C. Yang, J. Mun, S. Y. Kwon, S. Park, Z. Bao, S. Park, Electronic skin: Recent progress and future prospects for skin-attachable devices for health monitoring, robotics, and prosthetics. *Adv. Mater.* **31**, e1904765 (2019).
22. D. H. Ho, Q. Sun, S. Y. Kim, J. T. Han, D. H. Kim, J. H. Cho, Stretchable and multimodal all graphene electronic skin. *Adv. Mater.* **28**, 2601–2608 (2016).
23. S. Zhao, R. Zhu, Electronic skin with multifunction sensors based on thermosensation. *Adv. Mater.* **29**, 1606151 (2017).
24. G. Z. Li, R. Zhu, A multisensory tactile system for robotic hands to recognize objects. *Adv. Mater. Technol.* **4**, 1900602 (2019).
25. P. Delmas, J. Hao, L. Rodat-Despoix, Molecular mechanisms of mechanotransduction in mammalian sensory neurons. *Nat. Rev. Neurosci.* **12**, 139–153 (2011).
26. J. Dargahi, S. Najarian, Human tactile perception as a standard for artificial tactile sensing—A review. *Int. J. Med. Robotics Comput. Assist. Surg.* **1**, 23–35 (2004).
27. L. Wang, R. Zhu, G. Li, Temperature and strain compensation for flexible sensors based on thermosensation. *ACS Appl. Mater. Interfaces* **12**, 1953–1961 (2019).
28. S. Zhao, R. Zhu, A smart artificial finger with multisensations of matter, temperature, and proximity. *Adv. Mater. Technol.* **3**, 1800056 (2018).
29. S. Zhao, R. Zhu, Y. Fu, Piezothermic transduction of functional composite materials. *ACS Appl. Mater. Interfaces* **11**, 4588–4596 (2019).
30. R. Y. Que, R. Zhu, Q. Z. Wei, Z. Cao, Temperature compensation for thermal anemometers using temperature sensors independent of flow sensors. *Meas. Sci. Technol.* **22**, 085404 (2011).
31. S. Sundaram, P. Kellnhofer, Y. Li, J.-Y. Zhu, A. Torralba, W. Matusik, Learning the signatures of the human grasp using a scalable tactile glove. *Nature* **569**, 698–702 (2019).
32. S. S. Baishya, B. Bäuml, Robust material classification with a tactile skin using deep learning, in *2016 IEEE/RSJ International Conference on Intelligent Robots and Systems (IROS)* (2016), pp. 8–15.
33. Y. LeCun, Y. Bengio, G. Hinton, Deep learning. *Nature* **521**, 436–444 (2015).

34. A. Paszke, S. Gross, S. Chintala, G. Chanan, E. Yang, Z. DeVito, Z. Lin, A. Desmaison, L. Antiga, A. Lerer, Automatic differentiation in PyTorch, in *31st Conference on Neural Information Processing Systems (NIPS)* (2017), pp. 1–4.
35. L. J. Gibson, M. F. Ashby, *Cellular Solids: Structure & Properties*. (Cambridge Univ. Press, 1997).
36. P. Koistinen, L. Holmström, Kernel regression and backpropagation training with noise, in *Advances in Neural Information Processing Systems (NIPS)* (1992), pp. 1033–1039.
37. X. Peng, Z. Tang, F. Yang, R. S. Feris, D. Metaxas, Jointly optimize data augmentation and network training: Adversarial data augmentation in human pose estimation, in *Proceedings of the IEEE Conference on Computer Vision and Pattern Recognition (CVPR)* (2018), pp. 2226–2234.

**Acknowledgments:** We would like to thank J. Zhang for the helpful advice on the classification model training. **Funding:** This work was financially supported by National Key Research and Development Program of China (grant no. 2019YFB1310204), National Natural

Science Foundation of China (grant no. 51735007), and Beijing Natural Science Foundation (grant no. 3191001). **Author contributions:** R.Z. proposed the original idea. G.L. and R.Z. conceived and designed the sensor and robotic system. G.L. and S.L. designed the circuit system. G.L. and L.W. performed the experiments. G.L. and R.Z. co-wrote the manuscript.

**Competing interests:** The authors declare that they have no competing interests. **Data and materials availability:** All data needed to evaluate the conclusions of the paper are available in the paper or the Supplementary Materials.

Submitted 16 May 2020

Accepted 17 November 2020

Published 16 December 2020

10.1126/scirobotics.abc8134

**Citation:** G. Li, S. Liu, L. Wang, R. Zhu, Skin-inspired quadruple tactile sensors integrated on a robot hand enable object recognition. *Sci. Robot.* **5**, eabc8134 (2020).

# Science Robotics

## Skin-inspired quadruple tactile sensors integrated on a robot hand enable object recognition

Guozhen Li, Shiqiang Liu, Liangqi Wang and Rong Zhu

*Sci. Robotics* **5**, eabc8134.  
DOI: 10.1126/scirobotics.abc8134

ARTICLE TOOLS

<http://robotics.science.org/content/5/49/eabc8134>

SUPPLEMENTARY MATERIALS

<http://robotics.science.org/content/suppl/2020/12/14/5.49.eabc8134.DC1>

RELATED CONTENT

<http://robotics.science.org/content/robotics/5/49/eabf1502.full>  
<http://robotics.science.org/content/robotics/3/22/eaat0429.full>  
<http://robotics.science.org/content/robotics/3/24/eaau6914.full>

REFERENCES

This article cites 31 articles, 1 of which you can access for free  
<http://robotics.science.org/content/5/49/eabc8134#BIBL>

PERMISSIONS

<http://www.science.org/help/reprints-and-permissions>

Use of this article is subject to the [Terms of Service](#)

---

*Science Robotics* (ISSN 2470-9476) is published by the American Association for the Advancement of Science, 1200 New York Avenue NW, Washington, DC 20005. The title *Science Robotics* is a registered trademark of AAAS.

Copyright © 2020 The Authors, some rights reserved; exclusive licensee American Association for the Advancement of Science. No claim to original U.S. Government Works